

Article

The Effect of Sintering Oxygen Partial Pressure on a SmBiO₃ Buffer Layer for Coated Conductors via Chemical Solution Deposition

Xiaolei Zhu ¹, Yong Zhao ^{1,2,*}, Minghua Pu ¹, Yong Zhang ¹, Hong Zhang ¹ and Cuihua Cheng ²

¹ Key Laboratory of Advanced Technologies of Materials, Ministry of Education, Superconductivity and New Energy R&D Center, Southwest Jiaotong University, Chengdu, Sichuan 610031, China; zhuxiaolei578284@163.com (X.Z.); mhpu@home.swjtu.edu.cn (M.P.); yongzhang@home.swjtu.edu.cn (Y.Z.); zhanghong@home.swjtu.edu.cn (H.Z.)

² School of Materials Science and Engineering, University of New South Wales, Sydney, 2052 NSW, Australia; chengcecily@yahoo.com.au

* Correspondence: yzhaoh@home.swjtu.edu.cn. Tel.: +86-28-8760-0786

Academic Editor: Maria Miritello

Received: 15 August 2016; Accepted: 14 October 2016; Published: 21 October 2016

Abstract: The application of high-temperature YBa₂Cu₃O_{7-δ} (YBCO) superconducting material is a considerable prospect for the growing energy shortages. Here, SmBiO₃ (SBO) films were deposited on (100)-orientated yttrium-stabilized zirconia (YSZ) simple crystal substrates via the chemical solution deposition (CSD) approach for coated conductors, and the effects of sintering oxygen partial pressure on SBO films were studied. The crystalline structures and surface morphologies of SBO films were characterized by X-ray diffraction (XRD), scanning electron microscopy (SEM), and atomic force microscope (AFM). The optimized growth temperature, the intensity ratios of the SBO (200) peak to the SBO (111) peak, and the crystallinities of SBO films increased with the sintering oxygen partial pressure. The SEM and AFM images displayed a smooth and well-distributed surface in the argon atmosphere. The subsequent YBCO films with superconducting transition temperatures ($T_c = 89.5$ K, 90.2 K, and 86.2 K) and critical current densities ($J_c = 0.88$ MA/cm², 1.69 MA/cm², and 0.09 MA/cm²; 77 K, self-field) were deposited to further check the qualities of the SBO layer. These results indicated that sintering oxygen partial pressure had an effect on the epitaxial growth of the SBO buffer layer and YBCO superconducting properties. The experimental results may be a usable reference for the epitaxial growth of YBCO-coated conductors and other oxides.

Keywords: sintering oxygen partial pressure; epitaxial growth; chemical solution deposition; SmBiO₃ films

1. Introduction

As a kind of high-temperature superconducting material, YBa₂Cu₃O_{7-δ} (YBCO)-coated conductors may be more widely used in the future than Bi-based superconducting tapes because of its higher current-carrying capability and larger irreversibility fields [1]. However, the essential characteristics of superconducting weak coupling at the grain boundary require the deposition of YBCO films on biaxial textured flexible tape. Coated conductors are mainly composed of a textured substrate, a buffer layer, and a superconducting layer. So far, there are two practical routes to obtain textured substrates: rolling assisted biaxially textures (RABiTS) [2,3] and ion beam assisted deposition (IBAD) [4–6]. Ni-based alloy tape with yttrium-stabilized zirconia (YSZ) seed layer deposited via an IBAD route (named IBAD-YSZ tape) is a textured substrate suited for coated conductors [6]. The indispensable buffer layers are added between the substrate and the superconducting layer to provide an oxygen diffusion barrier for Ni and an oriented lattice-matched surface for YBCO epitaxial

growth. Thus, the quality of the buffer layer directly affects the structures and superconducting properties of coated conductors.

So far, the potential buffer materials for coated conductors have been prepared via physical and chemical approaches [7,8]. Chemical solution deposition (CSD) is a promising approach with such advantages as precise control and a low cost for fabricating YBCO-coated conductors [9,10]. The growth of the buffer layer prepared via CSD methods with traditional materials should be achieved at a relatively high sintering temperature of 900–1150 °C because of their high melting point [9]. In order to lower the sintering temperature of the buffer layer for coated conductors in CSD processing, a class of new buffer materials, REBiO₃ (RE correspond to a rare earth element), were developed, and their physical and chemical property were systematically characterized [11,12]. A REBiO₃ buffer layer can be epitaxially grown at a relatively low temperature of around 700–900 °C [12–17] because of its low formation temperature. Lowering the processing temperature not only means saving energy and reducing cost, but can also avoid or reduce some of the difficulties of manufacturing coated conductors, e.g., avoiding mechanical strength degradation at high temperatures for metal substrates and reducing chemical diffusion in the interface of the buffer layer and substrate. In addition, once formed, the REBiO₃ buffer layer possesses very good thermal stability as studied via thermal decomposition experiments in different oxygen partial pressures for YBiO₃ (YBO) precursor powders [13]. Taking these advantages, YBO and SmBiO₃ (SBO) films have been successfully grown in air [14,15]. GdBiO₃ (GBO) and DyBiO₃ (DBO) films have also been successfully grown in argon gas [16,17]. These studies also revealed that the optimal growth temperatures are different when different oxygen partial pressures are used for the buffer layer processing, and film qualities are also different.

However, these previous studies were carried out only under some individual condition; a more systematic study on the growth of REBO layers in various oxygen partial pressures should be carried out in order to optimize the processing condition and improve the quality of the buffer layer film. In addition, it is also necessary to figure out the effect of sintering oxygen partial pressure on the structural characteristics and surface morphology of REBiO₃ films. Since the lattice mismatches of SBO with YBCO and YSZ are 2% and 7%, respectively, SBO is a good choice for use as a buffer for making YBCO-coated conductors on an IBAD-YSZ Ni substrate. In this article, the epitaxial growth of SBO thin films sintered at different oxygen partial pressures via the CSD method on YSZ crystal substrates was systematically studied. YBCO epitaxial films were then grown on the buffer to further check the efficiency of SBO as a buffer layer for YBCO-coated conductors.

2. Materials and Methods

2.1. The Preparation of the SmBiO₃ Buffer Layer

The precursor solution was synthesized by dissolving samarium and bismuth nitrate (the molar ratio of Bi(NO₃)₃:Sm(NO₃)₃ = 1:1) in lactic acid at room temperature with constant stirring with a magnetic stirrer to achieve a light yellow solution. The cationic concentration of the solution was 0.6 mol/L. Then, the precursor solution was coated on a (100)-oriented YSZ single crystal substrate with a spinning rate of 3500 rpm via spin-coating. After that, the coated samples were placed in a preheated tube furnace at 120 °C for 30 min to remove the solvent of lactic acid. Subsequently, the dried samples were heated to 520 °C with a ramp rate of 80 K·min⁻¹, and the precursor films were obtained. Finally, the pyrolyzed films were crystallized at 700–900 °C in various atmospheres to form the (100)-oriented SBO layers.

2.2. The Preparation of YBa₂Cu₃O_{7-δ} Superconducting Layer

The subsequent YBCO superconducting layers were deposited on a SBO-buffered YSZ substrate with a fluorine-free CSD method [18] to check the quality of the SBO buffer layer. The YBCO precursor solution was synthesized by dissolving yttrium, barium, and copper acetates in propionic acid according to the stoichiometric quantity to achieve a dark green solution. Then, a certain amount

of polymer polyvinyl butyral (PVB) was incorporated to increase viscosity and homogeneity of the coating solution. The cationic concentration of the dark green solution was 0.9 mol/L. The YBCO precursor solution was coated on SBO-buffered substrates with a spinning rate of 5000–7000 rpm for 15 s. Then, the coated samples were heated at room temperature to 500 °C in a humid Ar and O₂ mixture to obtain nanocrystalline YBCO precursor films. The precursor films were first fired at 815–845 °C for several minutes and then annealed at 770 °C in dry argon gas for 1 h. Finally, the films were oxygenized at 450 °C for several hours to form a superconducting YBCO phase.

2.3. Characterization

The texture analyses including phi scan were performed by via X-ray diffraction (XRD, X' Pert PRO, PANalytical B.V, Almelo, The Netherlands). The microstructure analyses, as well as the cross-sectional investigation of the films, were performed with a scanning electron microscope (SEM, JSM-7001F, JEOL, Tokyo, Japan). The surface roughness of the films was investigated with an atomic force microscope (AFM, SPA-400, NSK, Tokyo, Japan). Superconducting transition and magnetic hysteretic loops were measured with a superconducting quantum interference device (SQUID) (Quantum-Design XL7, Quantum Design, Inc., San Diego, CA, USA). The critical current density was determined by the Bean critical state model formula [19] using the *M–H* curve.

3. Results and Discussion

The sintering oxygen partial pressures of air, argon, high-purity argon, and an Ar–H₂ gas mixture atmosphere correspond to 0.21 atm, 2×10^{-6} atm, 0.2×10^{-6} atm, and 2×10^{-10} atm, respectively [20]. The θ – 2θ XRD patterns of the SBO precursor films sintered at 700–900 °C in various atmospheres are shown in Figure 1. Only the SBO (200) and SBO (400) peaks were detected, besides the peaks of the YSZ substrate from the XRD patterns, which reveal that the strong (100)-oriented SBO films can be grown on YSZ substrates in air and argon atmosphere shown in Figure 1a,b. The SBO (200) and SBO (111) peaks appearing simultaneously in a high-purity argon atmosphere are shown in Figure 1c, which reveals the SBO crystalline grains with different orientations. However, the SBO (111) peaks were negligible. In addition, no peaks of SBO films were detected in Figure 1d. The inset showed that bismuth oxide was mainly reduced to bismuth, and the SBO film could not be obtained in an Ar–H₂ gas mixture. Therefore, a sintering atmosphere seriously affects the epitaxial growth of SBO films.

For simplicity, we denoted the optimized (100)-oriented SBO films sintered in air, argon, and high-purity argon as Sample A, Sample B, and Sample C. Figure 2 showed the XRD patterns of the optimized (100)-oriented SBO films sintered at different oxygen partial pressures. As a comparative analysis on film structure and quality, several aspects of samples sintered in different oxygen partial pressures are given in Table 1.

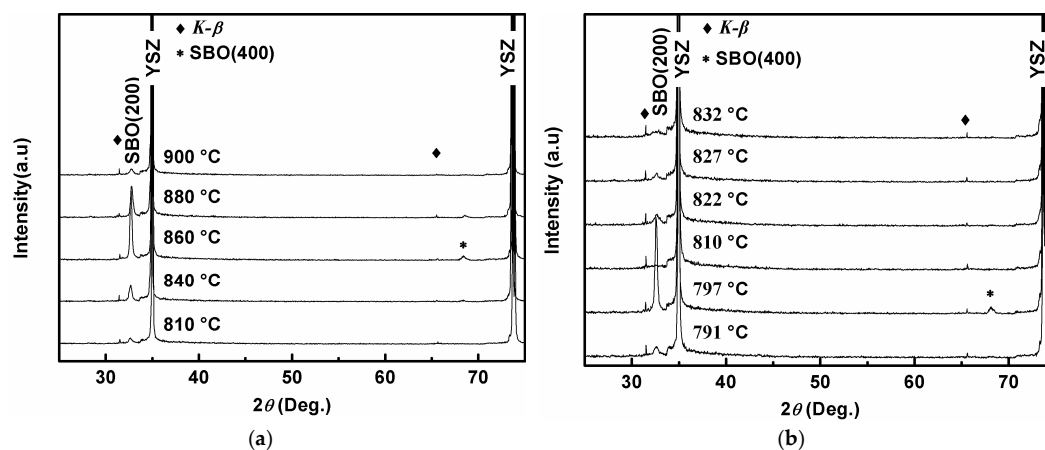


Figure 1. Cont.

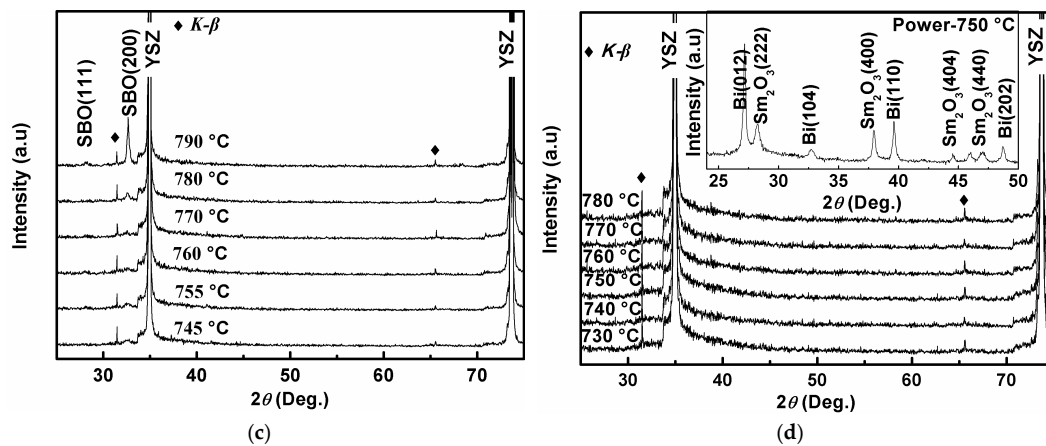


Figure 1. The θ - 2θ X-ray diffraction patterns of SmBiO_3 (SBO) films sintered in various atmospheres. (a) Air; (b) Argon (99.9 vol.% Ar-0.1 vol.% O_2); (c) High-purity argon (Ar-0.002 vol.% O_2); (d) Ar- H_2 gas mixture (Ar-4 vol.% H_2). The inset is the powder diffraction patterns of SBO precursor sintered in Ar- H_2 gas mixture.

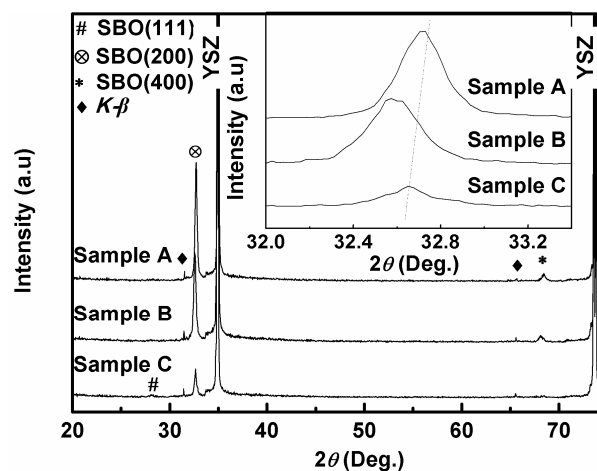


Figure 2. The θ - 2θ X-ray diffraction (XRD) patterns of the optimized (100)-oriented SBO films sintered in different oxygen partial pressures. The inset represents partial enlarged details of the optimized SBO films.

Table 1. The parameters of the optimized SBO films sintered in different oxygen partial pressures.

Oxygen Partial Pressure (atm)	Temperature and Time ($^{\circ}\text{C}$, min)	2θ Values of SBO(200) Peak ($^{\circ}$)	Grain Size (nm)
0.21 (Sample A)	860 $^{\circ}\text{C}$ -30 min	32.729 $^{\circ}$	38.77
2×10^{-6} (Sample B)	797 $^{\circ}\text{C}$ -60 min	32.589 $^{\circ}$	37.16
0.2×10^{-6} (Sample C)	780 $^{\circ}\text{C}$ -80 min	32.664 $^{\circ}$	38.74

From Table 1, we can clearly see that Sample A, Sample B, and Sample C were obtained with the optimized temperature and time of, respectively, 860 $^{\circ}\text{C}$ and 30 min, 797 $^{\circ}\text{C}$ and 60 min, and 780 $^{\circ}\text{C}$ and 80 min. Higher oxygen partial pressures corresponded to higher temperatures and shorter times for epitaxial growth. The possible explanations for these results are that, at first, a lower oxygen partial pressure and a higher sintering temperature provides a good condition for reducing bismuth oxide, which is harmful for the formation of SBO. Therefore, under a relatively low oxygen partial pressure, a lower sintering temperature is necessary to match the phase formation and support the phase thermal stability of SBO. However, a lower temperature may also reduce the crystal growth rate. This is why under a lower oxygen partial pressure, an optimal sintering temperature is lower

and the sintering time is longer. On the contrary, under a relatively high oxygen partial pressure, bismuth oxide can afford a relatively high sintering temperature before being reduced. Moreover, a higher temperature is helpful for the crystal growth.

By the Scherrer formula [21], the average grain sizes of the SBO were calculated and are shown in Table 1. The grain sizes of SBO obtained at the different oxygen partial pressures were 38.77 nm, 37.16 nm, and 38.74 nm. There were few differences in the grain sizes obtained at different oxygen partial pressures. The grain sizes of the crystallization phenomenon are associated with the sintering temperature and time, and a higher growth temperature with an increasing driving force needs less time for adequate crystallization.

In addition, the shift of the SBO (200) peak toward a higher diffraction angle, from 32.582° to 32.726° , indicated a decrease in the lattice constant, which stemmed from the minimal volatile constituent of Bi_2O_3 from the surface at 860°C in air (the melting point of Bi_2O_3 is 824°C). Meanwhile, the shift of the SBO (200) peak toward a higher diffraction angle from 32.582° to 32.664° may stem from the increase in defect in the SBO film sintered in a high-purity argon atmosphere.

Besides, there were still some other significant differences in the crystallographic orientation and structure of the SBO epitaxial film. Figure 3a shows the intensity ratios of the SBO (200) peak to the SBO (111) peak sintered at different oxygen partial pressures. As a function to evaluate the (100)-crystallographic orientation, the corresponding values of Sample A, Sample B, and Sample C were 161.4, 76.96, and 13.99, respectively, and these values indicate that (100)-crystallographic orientation increased with sintering oxygen partial pressure. Figure 3b shows the out-of-plane textures of epitaxial films via phi scan from the SBO (111) peak. The four equally spaced diffraction peaks imply that SBO has a cubic structure. The SBO films were grown directly on the YSZ substrate. The values of the full width at half maximum (FWHM)— 1.188° , 1.477° , and 1.604° —display an increase in the crystallinity of the SBO films with the sintering oxygen partial pressure. The higher oxygen partial pressures correspond to the higher growth temperatures. The atomic diffusion at higher temperatures is fast and adequate, while the diffusion at lower temperatures suppresses the formation of the SBO phase.

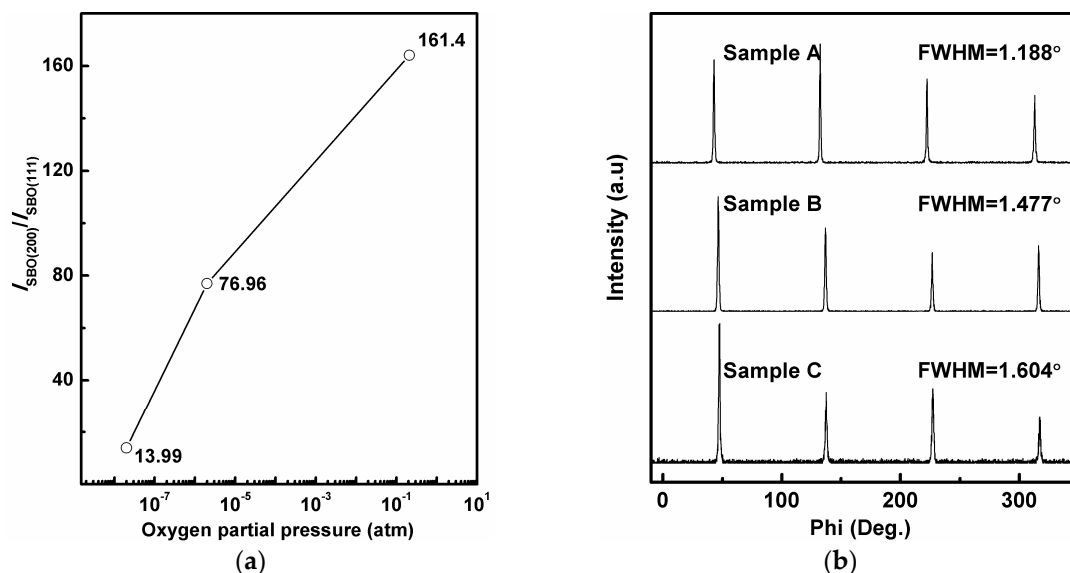


Figure 3. The optimized SBO films sintered in different oxygen partial pressures. (a) The intensity ratios of the SBO (200) peak to the SBO (111) peak; (b) The normalized phi scans from the SBO (111) peak.

As an important factor, the surface morphologies of the buffer layer affect the superconductivity of the subsequent superconducting layer. The surface morphologies of the SBO films sintered at different oxygen partial pressures were investigated via SEM and AFM. Figure 4 shows the SEM images of Sample A, Sample B, and Sample C. There was an undulating shape surface observed on Sample A

in Figure 4a, which was generated by the minimal aggregation and volatilization of Bi_2O_3 . However, the smooth surfaces without significant holes or cracks in the magnified images were obtained from Sample B in Figure 4b and Sample C in Figure 4c. The atomic ratio of Sm:Bi via EDS analysis of Sample B in Figure 4b was 1:0.84, which suggests that the crystal structure of the SBO layer was still cubic $\text{Sm}_{1-x}\text{Bi}_x\text{O}_{1.5}$ [12]. The AFM images of the SBO epitaxial films sintered at different oxygen partial pressures are shown in Figure 5. The surface morphologies of the different SBO epitaxial films correspond to the root mean square roughness (RMS) values of 2.631 nm, 0.8229 nm, and 2.54 nm over an area of $4\ \mu\text{m} \times 4\ \mu\text{m}$ in Figure 5a–c. The surface morphologies of the SBO films first decreased and then increased with sintering oxygen partial pressures. The surface roughness of the SBO films at high growth temperatures was increased by the minimal aggregation and volatilization of Bi_2O_3 . Conversely, the crystallinities of the SBO film were decreased, and the surface roughness was increased at low sintering oxygen partial pressures by the low diffusion rates. The equilibrium among the film quality (morphology and microstructure), the high temperature cost, and the excessive oxidation of Ni alloy tape is very important for the SBO buffer layer of coated conductors.

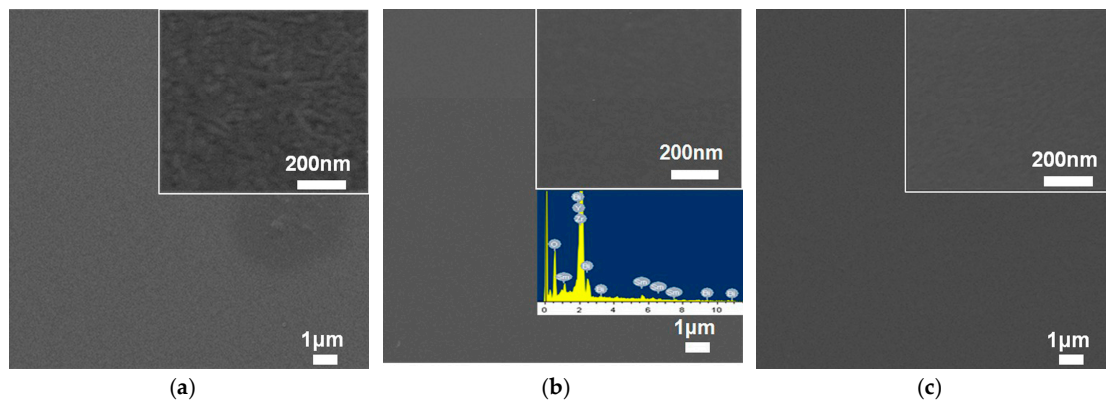


Figure 4. The SEM images of SBO epitaxial films sintered in different oxygen partial pressures. (a) Sample A; (b) Sample B; (c) Sample C. The inset: The magnified surfaces of SBO epitaxial films.

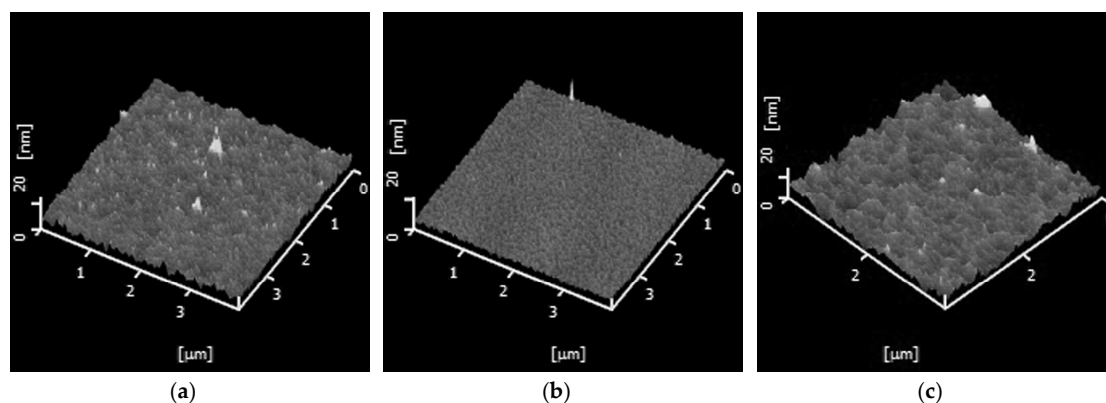


Figure 5. The AFM images of SBO epitaxial films grown in different oxygen partial pressures. (a) Sample A; (b) Sample B; (c) Sample C. ($4\ \mu\text{m} \times 4\ \mu\text{m}$).

The YBCO superconducting layers were deposited on SBO/YSZ samples, which were used to check the qualities of the SBO film obtained at different oxygen partial pressures. Figure 6 shows the θ - 2θ XRD patterns of the YBCO films on different samples. The more obvious YBCO (001) diffraction peaks from the YBCO films on Sample B, compared with those on Samples A and C, illustrated a highly *c*-axis orientation. However, the diffraction peak at around 29.5° revealed some impurity, generated at the interface of the SBO and YBCO layers (Sm_2O_3 and Bi_2O_3 reacted with BaO to form

SmBa₂BiO₆). The different intensities of impure SmBa₂BiO₆ (220) peaks in different samples implied the differences in the extent of oxide reaction, which were related to the microstructures and surface morphologies of the SBO buffer layer. The smooth and dense surface without obvious undulation can suppress SmBa₂BiO₆ formation. Therefore, the sintering oxygen partial pressure indirectly affects YBCO epitaxial growth.

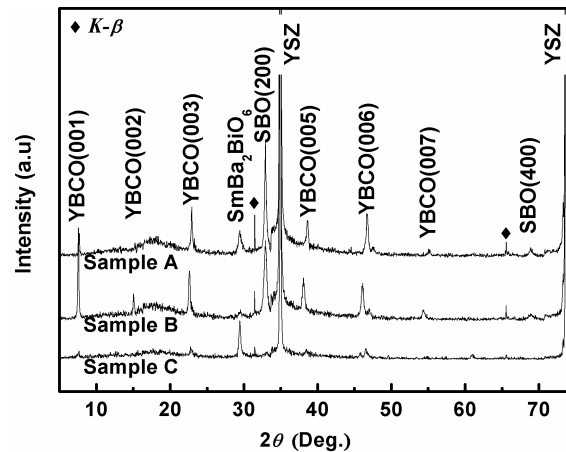


Figure 6. The θ - 2θ X-ray diffraction patterns of YBa₂Cu₃O_{7- δ} (YBCO) films on different samples.

Figure 7 shows the superconducting properties of YBCO films. The superconducting transition temperatures (T_c) of YBCO films on Sample A, Sample B, and Sample C were 89.5 K, 90.2 K, and 86.2 K, respectively. In addition to this, the YBCO film of Sample B in Figure 7a presented a sharper superconducting transition and a stronger diamagnetic signal than those of Samples A and C, which demonstrated a purer YBCO phase and higher superconducting transition temperatures. Figure 7b shows the current density versus the magnetic field of YBCO films at 77 K on different samples. The critical current density (J_c) values of the YBCO films on Sample A, Sample B, and Sample C were 0.88 MA/cm², 1.69 MA/cm², and 0.09 MA/cm² (77 K, self-field), respectively. The different superconducting properties of the YBCO films may stem from the qualities of the SBO film and the new production of SmBa₂BiO₆ impurity at the interface. Thus, a smooth, dense surface of the SBO film sintered in an argon atmosphere is the best alternative for subsequent YBCO superconducting layers. In future work, we will optimize the preparation parameters of YBCO films and introduce artificial pinning centers to further improve the current-carrying capability of YBCO coated conductors.

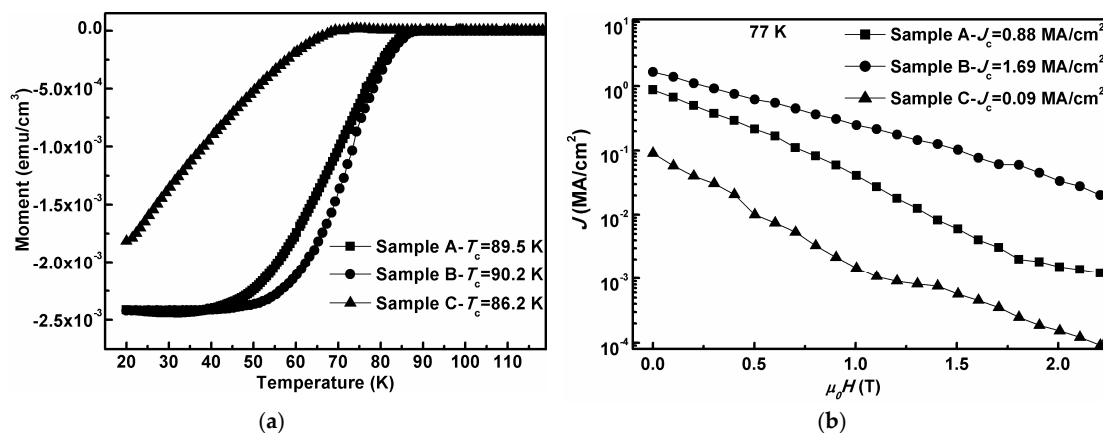


Figure 7. The superconducting properties of YBCO films on different samples. (a) The magnetic moment versus the temperature for YBCO coated conductors; (b) the current density versus the magnetic field at 77 K.

4. Conclusions

SBO buffer layers sintered in different oxygen partial pressures on (100)-oriented YSZ simple crystal substrates were obtained via the CSD methods, and the effect of the sintering oxygen partial pressure on SBO buffer layers was systematically discussed. The results show that the sintering oxygen partial pressure has an important effect on film quality. The higher sintering oxygen partial pressures corresponded to the higher growth temperature and shorter time. The intensity ratios of the SBO (200) peak to the SBO (111) peak, and the crystallinities of SBO films, increased with sintering oxygen partial pressure. The SEM and AFM images displayed the smooth and well-distributed surface sintered in the argon atmosphere. The subsequent YBCO superconducting layers on different samples were deposited to further check the qualities of the SBO buffer layers; the different superconducting properties of YBCO films may stem from the quality of the SBO film. The sintering oxygen partial pressure directly and indirectly affected the epitaxial growth of the SBO buffer layer and the superconducting properties of the YBCO superconducting layer.

Acknowledgments: This work was supported by the National Natural Science Foundation of China (Grant No. 51072168; 51377138), the Program of International S&T Cooperation under Grant (Grant No. 2013DFA51050); the 863 Program (Grant No. 2014AA032701); the Fundamental Research Funds for the Central Universities (A0920502051411-5), and the 2013 Doctoral Innovation Funds of Southwest Jiaotong University.

Author Contributions: Yong Zhao and Minghua Pu conceived and designed the experiments; Xiaolei Zhu performed the experiments; Xiaolei Zhu, Hong Zhang and Yong Zhang analyzed the data; Yong Zhao contributed reagents/materials/analysis tools; Xiaolei Zhu and Cuihua Cheng wrote the paper.

Conflicts of Interest: The authors declare no conflict of interest.

References

1. Obradors, X.; Puig, T. Coated conductors for power applications: Materials challenges. *Supercond. Sci. Technol.* **2014**, *27*, 98–102. [[CrossRef](#)]
2. Doi, T.J.; Yuasa, T.; Ozawa, T.; Higashiyama, K. Transport critical current densities in uniaxially and biaxially oriented $Tl_1(Ba_{0.8}Sr_{0.2})_2Ca_2Cu_3O_9$ superconducting films on Ag and $SrTiO_3$ substrates prepared by a spray decomposition method. *Jpn. J. Appl. Phys. Part 1* **1994**, *33*, 5692–5696. [[CrossRef](#)]
3. Goyal, A.; Lee, D.F.; List, F.A.; Specht, E.D.; Feenstra, R.; Paranthaman, M.; Cui, X.; Lu, S.W.; Martin, P.M.; Kroeger, D.M.; et al. Recent progress in the fabrication of high- J_c tapes by epitaxial deposition of YBCO on RABiTS. *Physica C* **2001**, *357*, 903–913. [[CrossRef](#)]
4. Iijima, Y.; Tanabe, N.; Kohno, O.; Ikeno, Y. Biaxially aligned $YBa_2Cu_3O_{7-\delta}$ thin film tapes. *Physica C Supercond.* **1991**, *185*, 1959–1960. [[CrossRef](#)]
5. Rupich, M.W.; Li, Q.; Annavarapu, S.; Thieme, C.; Zhang, W.; Prunier, V.; Paranthaman, M.; Goyal, A.; Lee, D.F.; Specht, E.D.; et al. Low cost Y-Ba-Cu-O coated conductors. *IEEE Trans. Appl. Supercond.* **2001**, *11*, 2927–2930. [[CrossRef](#)]
6. Iijima, Y.; Tanabe, N.; Kohno, O.; Ikeno, Y. In-plane aligned $YBa_2Cu_3O_{7-\delta}$ thin films deposited on polycrystalline metallic substrates. *Appl. Phys. Lett.* **1992**, *60*, 769–771. [[CrossRef](#)]
7. Obradors, X.; Puig, T.; Pomar, A.; Sandiumenge, F.; Mestres, N.; Coll, M. Progress towards all-chemical superconducting $YBa_2Cu_3O_7$ -coated conductors. *Sci. Technol.* **2006**, *19*, S13–S26. [[CrossRef](#)]
8. Wang, B.B.; Liu, L.F.; Wu, X.; Yao, Y.J.; Wang, M.L.; Lu, S.D. Surface morphology of cerium oxide layer and its effect on the performance of superconducting layer. *J. Supercond. Nov. Magn.* **2016**, *29*, 1–8. [[CrossRef](#)]
9. Schwartz, R.W.; Schneller, T.; Waser, R. Chemical solution deposition of electronic oxide films. *C. R. Chim.* **2004**, *7*, 433–461. [[CrossRef](#)]
10. Ghasemi, A.; Ashrafizadeh, F.; Golozar, M.A. Optimisation of processing parameters on formation of silica coating on nickel substrates by sol-gel processing. *Surf. Eng.* **2013**, *21*, 131–138. [[CrossRef](#)]
11. Zhao, Y.; Pu, M.H.; Li, G.; Du, X.H.; Zhou, H.M.; Zhang, Y.B.; Yang, X.S.; Wang, Y.; Sun, R.P.; Cheng, C.H. Development of a new series of buffer layers for REBCO coated conductors. *Physica C* **2007**, *463*, 574–579. [[CrossRef](#)]
12. Bellakki, M.B.; Prakash, A.S.; Shivakumara, C.; Hegde, M.S.; Shukla, A.K. Solution-combustion synthesis of $Bi_{1-x}Ln_xO_{1.5}$ ($Ln = Y$ and $La-Yb$) oxide ion conductors. *Bull. Mater. Sci.* **2006**, *29*, 339–345. [[CrossRef](#)]

13. Pollefeyt, G.; Rottiers, S.; Vermeir, P.; Lommens, P.; Hühne, R.; Buysser, K.D.; Driessche, I.V. Feasibility study of the synthesis of YBiO₃ thin films by aqueous chemical solution deposition as an alternative for CeO₂ buffer layers in coated conductors. *J. Mater. Chem. A* **2013**, *1*, 3613–3619. [[CrossRef](#)]
14. Li, G.; Pu, M.H.; Du, X.H.; Zhou, H.M.; Zhao, Y. A new single buffer layer for YBCO coated conductors prepared by chemical solution deposition. *Physica C* **2007**, *452*, 43–47. [[CrossRef](#)]
15. Li, G.; Pu, M.H.; Zhou, H.M.; Du, X.H.; Zhao, Y. Possible new single-buffer layers for YBa₂Cu₃O_{7-y} coated conductors prepared by chemical solution deposition. *J. Mater. Res.* **2007**, *22*, 2398–2403. [[CrossRef](#)]
16. Wang, Z.Q.; Pu, M.H.; Mu, L.Y.; Sun, R.P.; Li, G.; Wang, W.T.; Bai, Y.Q.; Zhao, Y. Effect of annealing condition growth of GdBiO₃ film prepared by chemical solution deposition. *Cryo. Supercond.* **2008**, *36*, 36–39.
17. Sun, R.P.; Li, G.; Pu, M.H.; Wang, W.T.; Zhang, Y. Low temperature processing technology for preparation of potential DyBiO₃ buffer layers of coated conductors. *Rare. Metal. Mat. Eng.* **2009**, *38*, 901–904.
18. Wang, W.T.; Pu, M.H.; Wang, W.; Zhang, H.; Cheng, C.H.; Zhao, Y. Influence of partial melting temperature on structure and superconducting properties of YBCO film by non-fluorine MOD. *J. Supercond. Nov. Magn.* **2010**, *23*, 989–993. [[CrossRef](#)]
19. Gyorgy, E.M.; Van Dover, R.B.; Jackson, K.A.; Schneemeyer, L.F.; Waszczak, J.V. Anisotropic critical currents in Ba₂YCu₃O₇ analyzed using an extended Bean model. *Appl. Phys. Lett.* **1989**, *55*, 283–285. [[CrossRef](#)]
20. High_purity-gas/Ar. Available online: http://www.kodi.cn/GetKnowledge/zh-CN/High_purity_gas/Ar.aspx (accessed on 17 October 2016).
21. Patterson, A.L. The scherrer formula for X-ray particle size determination. *Phys. Rev.* **1939**, *56*, 978–982. [[CrossRef](#)]



© 2016 by the authors; licensee MDPI, Basel, Switzerland. This article is an open access article distributed under the terms and conditions of the Creative Commons Attribution (CC-BY) license (<http://creativecommons.org/licenses/by/4.0/>).